JOURNAL OF GEOPHYSICAL RESEARCH, VOL. 105, NO. D11, PAGES 14,891–14,898, JUNE 16, 2000

Comparison of model and observed regional temperature changes during the past 40 years

Gary L. Russell, James R. Miller, David Rind, Reto A. Ruedy, Gavin A. Schmidt, and Sukeshi Sheth

NASA Goddard Institute for Space Studies, New York

Abstract. Results are presented for six simulations of the Goddard Institute for Space Studies (GISS) global atmosphere-ocean model for the years 1950–2099. There are two control simulations with constant 1950 atmospheric composition from different initial states, two greenhouse gas (GHG) experiments with observed greenhouse gases up to 1990 and compounded 0.5% CO_2 annual increases thereafter, and two greenhouse gas plus sulfate (GHG + SO_4) experiments with the same varying greenhouse gases plus varying tropospheric sulfate aerosols. Surface air temperature trends in the two GHG experiments (with the control simulations climate drift subtracted out) are compared between themselves and with changes in the observed temperature record between 1960 and 1998. All comparisons show high positive spatial correlation in the Northern Hemisphere except in summer when the greenhouse signal is weakest. The GHG + SO_4 experiments show weaker correlations. In the Southern Hemisphere, correlations between any experiments or observations are either weak or negative, in part because the model's interannual variability of southern sea ice cover is unrealistic. The model results imply that temperature changes due to forcing by increased greenhouse gases have risen above the level of regional interannual temperature variability in the Northern Hemisphere over the past 40 years. This period is thus an important test of the reliability of coupled climate models.

1. Introduction

Atmosphere-ocean models must be tested against current climate, climate variability, and observed climate changes if their projections into the future are to have credibility. Numerous studies have compared global and hemispheric annual surface air temperature changes between model output and observations for the past century [*Tett et al*., 1999; *Delworth and Knutson*, 2000]. Many of them concluded that tropospheric sulfate aerosols must be added to greenhouse gas (GHG) simulations in order to improve the comparisons with observations.

Fewer studies have compared the spatial patterns of surface air temperature changes between realistic model simulations and observations. *Mitchell et al*. [1995] compared spatial correlation coefficients between model and observed decadal temperature changes relative to a 130-year mean. Their 15° spatial and annual averaging smoothed out some of the noise but also some of the signal, yet global correlation coefficients of ~0.3 occurred for a greenhouse gas simulation in the 1950s and a greenhouse gas and sulfate simulation in the 1970s and 1980s.

Knutson et al. [1999] examined interannual variability using several coupled model simulations from the Geophysical Fluid Dynamics Laboratory. Their simulations include realistic forcing from greenhouse gas increases and sulfate aerosols for the past 50 years. They compared global annual surface air temperature changes with observations and displayed seasonal spatial patterns of their simulations. Their R30 model simulations and the observations show cooling in the North Atlantic in all seasons and the greatest warming over northern Asia in winter.

Paper number 2000JD900156.
0148-0227/00/2000JD900156$09.00

Surface air temperature changes since 1950 are the best documented long-term observations [*Hansen et al*., 1996, 1999] with which climate models can be compared. They show clear regional patterns of change, although it is not yet certain whether these changes exceed the range of regional temperature variability. If a climate model simulation with realistic anthropogenic forcing can match the regional patterns of observed changes, it provides support for the detection and attribution of global climate change as well as validating the climate model's projections into the future.

The present study examines four global climate model experiments with realistic greenhouse gas increases, two of which contain sulfate aerosol changes, and compares them with observed changes for the past 39 years. To quantify the present model's skill in simulating regional changes in surface air temperature, spatial correlation coefficients are calculated among the model and observed data sets for each hemisphere and each season.

2. NASA Goddard Institute for Space Studies Atmosphere-Ocean Model With Improvements

The atmosphere-ocean model was developed at the Goddard Institute for Space Studies (GISS) by *Russell et al*. [1995]. There are nine vertical layers in the atmosphere and up to 13 in the ocean. The grid box horizontal resolution is 4° latitude by 5° longitude. The resolution for heat, water vapor, and salt is finer than the grid resolution because those quantities have both means and prognostic directional gradients inside each grid box. This information is used in the advection by the linear upstream scheme, and atmospheric condensation and ocean vertical mixing are performed on 2° by 2.5° horizontal resolution.

Several changes and improvements have been made to the

model since it was published. The ground hydrology scheme of *Abramopoulos et al*. [1988] replaced the old two-layer ground model. The conduction of heat through sea ice and glacial ice has been improved by replacing the old two-layer scheme with a four-layer scheme. Sea ice is now advected [*Miller and Russell*, 1997]. The inclusion of glacial ice calving off Antarctica helped to increase the Southern Ocean ice cover and to reduce water loss to the ice sheets. The former nonentraining convection and Richardson number dependent scheme for ocean vertical mixing has been replaced by the k profile parameterization (KPP) scheme of *Large et al*. [1994]. This improvement increased the Atlantic heat transport, which allowed a stable sea ice cover in the Northern Hemisphere and reduced the temperature drift in the North Atlantic.

3. Model Simulations

Starting from an observed atmospheric state, zero ocean currents, and climatological ocean temperature and salinity distributions [*Levitus et al*., 1994], the atmosphere-ocean model was spun up for 40 simulated years with constant 1950 atmospheric composition. From this spin up state, three simulations were integrated from 1950 to 2099: a control simulation that continues the spin up run, GHG1 experiment with observed greenhouse gases up to 1990 and compounded 0.5% CO_2 annual increases thereafter, and GHG + $SO_4$1 experiment with the same varying greenhouse gases plus varying tropospheric sulfate aerosols.

The control simulation had a significant climate drift in its surface air temperature amounting to 0.5°C in its first 60 years but <0.1°C for the last 90 years. This 0.5°C warming is comparable to the temperature separation between the control and GHG1 after the first 60 years.

Partly because of the climate drift problem and partly because GHG1 experiment reproduced the observed temperature changes from 1960 to 1998 well, three additional simulations were integrated: a new control simulation with 1950 atmospheric composition, a new GHG2 experiment, and a new GHG + $SO_4$2 experiment. The initial state for these new simulations was the state of the previous control after 60 years, or 100 years of integration from *Levitus et al*.'s [1994] observed ocean state. GHG2 and GHG + $SO_4$2 experiments also include chlorofluorocarbons in addition to F11 and F12, whereas the old experiments did not. By 1990 the additional chlorofluorocarbons have 60% of the radiative effect of F11 or 2% of the total greenhouse gas forcing since 1950. We use the term GHGs ensemble or GHG + SO_4s ensemble for the average of the two GHG experiments or of the two GHG + SO_4 experiments.

The tropospheric sulfate aerosol amounts used in the GHG + SO_4 experiments are from *Mitchell et al*. [1995], who provided two normalized sulfate loading patterns and global annual amounts for each pattern. The first pattern has the greatest aerosol concentration in central Europe and local maxima in the eastern United States and eastern China. The second pattern has a strong maximum in eastern China and weaker maxima in India, Turkey, southern Africa, and Mexico. Before 1991 the first pattern is used exclusively; after 2049 the second pattern is used exclusively; and from 1991 to 2049 a combination of the patterns is used. The radiative effect of the sulfate aerosol forcing is scaled so that from 1850 to 1990 the net radiative forcing is 0.9 W m^{-2} [*Houghton et al*., 1994, Figure 4.8].

When greenhouse gases are added to the Earth's atmosphere, the planet does not change discontinuously but strives to achieve a new equilibrium over time. At any instant in time the difference between the current state and the potential equilibrium based on the current atmospheric composition can be measured in terms of an unrealized radiative forcing. We theoretically estimate that in the real world, approximately half of the surface temperature changes due to greenhouse gas additions from 1850 to 1950 should have been realized by 1950 and half unrealized [*Hansen et al*., 1985].

Hansen et al. [1988] provided formulas to calculate the global surface air temperature change that would be required to maintain energy balance with space if no climate feedbacks occurred. Assuming that the CO_2 concentration was 285 ppm in 1850, these formulas estimate that the radiative forcing of greenhouse gases from 1850 to 1950 excluding feedbacks would be 0.21°C. The climate amplification factor of a prior version of the model (before the KPP ocean vertical mixing scheme was implemented) was estimated to be 2.2 (A. Sokolov and P. Stone, personal communication, 1999). The model GHG experiments were not integrated from 1850 to 1950, but had they been started in 1850, we estimate there would have been an unrealized warming by 1950 of $0.21 \times 2.2/2 = 0.23$°C. For the increasing tropospheric sulfate aerosol experiments the unrealized warming would have been <0.23°C.

We fit the global observed surface air temperature data from 1858 to 1998 [*Hansen et al*., 1999] by the least squares fit exponential of the form $A + B \exp(C \cdot \text{time})$. Subtracting the exponential fit from the observed temperature record, we see that the 1930s (0.11°C) and 1940s (0.11°C) were the warmest decades of the twentieth century relative to their atmospheric gas compositions. Regardless of the reason, after 1950 the real world behaved as though much of its possible unrealized warming from 1850 to 1950 had been realized during the 1930s and 1940s. Thus, starting the model experiments from cold start mode in 1950 and comparing with observed surface temperatures, we would estimate an effective unrealized temperature disparity (causing the model to be colder than the observations) to be <0.23°C. Because model results are warmer than the observations for the first 30 years, there is no clear evidence of a cold start problem. The model results are not modified for this unclear temperature disparity due to unrealized warming.

When compared with the real world, the atmosphere-ocean model's climate variables have errors of various magnitude in different seasons and locations. In addition, the ocean prognostic variables show systematic climate drifts of various magnitude. Thus the model's climate predictions should be based on differences between experiments and control simulations in order to reduce deviations from observations and for the same time periods in order to reduce climate drift. The model's climate changes are then based on atmospheric composition changes since 1950, the year whose fixed composition is used in the controls.

4. Comparison of Model and Observed Temperature Changes

Plate 1 shows the changes in global annual surface air temperature since 1950. The observed changes are measured relative to a constant 21-year average from 1940 to 1960. The model's changes are relative to a centered 21-year moving average of the appropriate control simulation. The moving

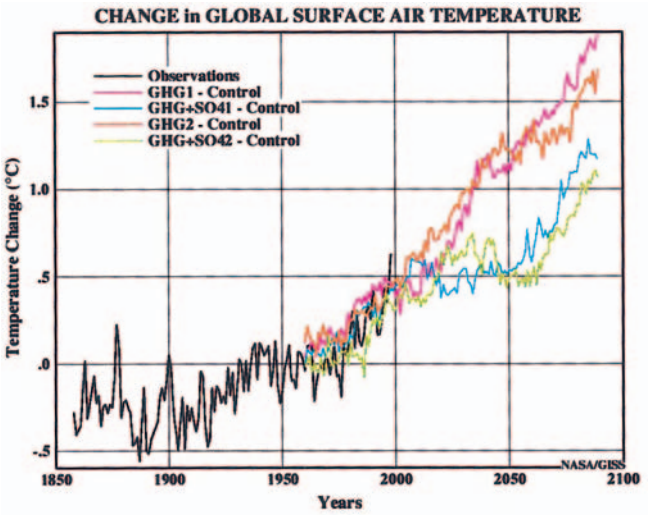

Plate 1. Change in global annual surface air temperature (°C) since 1950 for observations of *Hansen et al*. [1999] and four model experiments. The observations are relative to a constant 21-year average from 1940 to 1960. The experiment values are relative to centered 21-year moving averages of the appropriate control simulations.

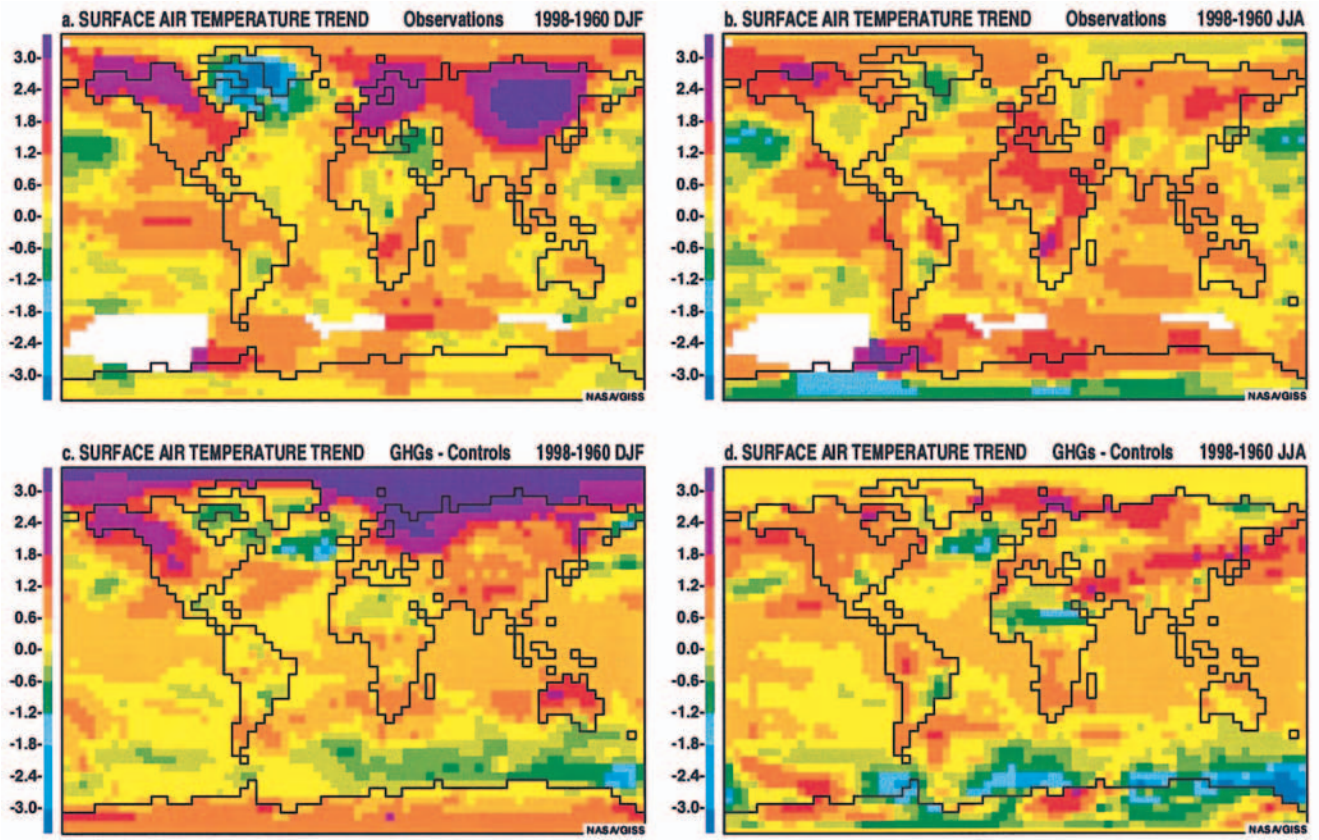

Plate 2. Winter and summer surface air temperature trends (°C) from 1960 to 1998 for the observations of *Hansen et al*. [1996] and the GHGs ensemble.

Table 1. Area-Weighted Spatial Correlation Coefficients of Surface Air Temperature Trends From 1960 to 1998 Between Observations and Model Experiments for Each Hemisphere and Each Season

	Northern Hemisphere				Southern Hemisphere			
	DJF	MAM	JJA	SON	DJF	MAM	JJA	SON
Obs. versus GHGs	0.454	0.591	0.005	0.220	−0.023	0.165	−0.097	0.142
Obs. versus GHG1	0.370	0.232	−0.109	0.198	0.056	0.145	0.049	0.081
Obs. versus GHG2	0.364	0.639	0.113	0.188	−0.057	0.047	−0.113	0.090
Obs. versus SO_4s	0.096	0.050	0.036	0.076	−0.057	0.111	−0.016	−0.109
Obs. versus $SO_4$1	0.058	0.008	0.001	0.012	−0.017	0.178	0.027	−0.156
Obs. versus $SO_4$2	0.091	0.072	0.049	0.093	−0.064	−0.031	−0.048	0.030
GHG1 versus GHG2	0.289	0.204	−0.009	0.524	−0.472	−0.484	−0.395	−0.321
$SO_4$1 versus $SO_4$2	0.264	0.277	0.229	0.004	−0.114	−0.050	−0.057	−0.141

GHGs is the ensemble average of the two GHG experiments. DJF, December–January–February; MAM, March–April–May; JJA, June–July–August; SON, September–October–November. Obs., observations.

subtraction reduces climate drift, and-the 21-year averaging allows Plate 1 to show each experiment's proper interannual variability. The model's variability is weaker than that of the observations in part because the experiments lack volcanic eruptions, insolation changes, and ozone changes that occurred in the real world.

For each year, each season, and each grid box a centered 21-year moving average of the appropriate control is subtracted from the surface air temperature of each model experiment in order to reduce the influence of climate drift. Next, for each season and each grid box the least squares fit line is calculated that fits the temperature changes for the 39 yearly points from 1960 to 1998. The temperature trend is defined as the slope of the line multiplied by 38 years. The least squares fit lines and temperature trends are also calculated for the observations [*Hansen et al*., 1996, 1999] which were spatially interpolated to the model's grid. Plate 2 shows, for winter and summer, the spatial distribution of temperature trends from 1960 to 1998 for the observations and the GHGs ensemble.

Cooling regions that are common to both the observations and the GHGs ensemble are the North Atlantic, Baffin Bay, the midlatitude Pacific Ocean, southern Greenland, southern Brazil, north central Africa in winter, and central United States in summer. Common regions of ocean warming are the tropical Pacific and Indian Oceans. Alaska, western Canada, and Eurasia are significantly warmer in winter but less so in summer. The model's poor simulation of El Niño at the current resolution causes the model to underestimate the observed warming in the tropical eastern Pacific.

The largest difference between GHG1 and GHG2 is that GHG1 shows significant warming in high southern latitudes, while GHG2 shows cooling there. The North Atlantic cooling is on the western side in GHG1 but on the eastern side in GHG2. Hudson Bay, Baffin Bay, and eastern Siberia show cooling in all seasons in GHG1 where GHG2 shows warming. Both GHG experiments show some cooling in the midlatitude oceans.

The causes of North Atlantic cooling were discussed by *Russell and Rind* [1999] using an earlier version of the atmosphere-ocean model. They found that increased poleward heat transport by the atmosphere reduces the poleward heat transport by the Atlantic Ocean, and Atlantic temperatures decline where formerly significant heat transport was received.

Hansen et al. [1996] speculated that the observed changes in temperature, particularly the winter cooling in Baffin Bay, Greenland, and the North Atlantic, could arise from unforced variability. The GHG experiments shown here indicate that the cooling in these regions appears to be caused by greenhouse gas forcing. The model results arise partially because increased greenhouse gases lead to heating over land, while reduced ocean heat transports produce cooler temperatures in the North Atlantic.

The mechanisms described here involve thermodynamic trace gas forcing (which warms the land more rapidly) and ocean heat transport changes (which are strongest in the North Atlantic). This is distinctly different from temperature changes due to atmospheric advection changes that occur in conjunction with variations in sea level pressure. Changes in the Arctic Oscillation (AO), the leading mode of Northern Hemisphere sea level pressure variability [*Thompson and Wallace*, 1998],

Table 2. Area-Weighted Spatial Correlation Coefficients of Surface Air Temperature Trends Between Observations and Model Experiments for Each Season for the Northern Hemisphere Excluding the Arctic Ocean but Including Greenland-Iceland-Norwegian Sea

	1960–1998				1950–1998			
	DJF	MAM	JJA	SON	DJF	MAM	JJA	SON
Obs. versus GHGs	0.537	0.517	0.009	0.149	0.485	0.525	−0.009	0.092
Obs. versus GHG1	0.380	0.108	−0.117	0.099	0.201	0.179	−0.084	0.165
Obs. versus GHG2	0.376	0.569	0.127	0.135	0.456	0.521	0.070	0.004
Obs. versus SO_4s	0.107	0.005	0.049	0.084	0.097	−0.079	0.070	0.064
Obs. versus $SO_4$1	0.076	0.027	0.017	0.067	−0.026	−0.017	0.108	0.090
Obs. versus $SO_4$2	0.091	−0.017	0.055	0.052	0.165	−0.107	0.017	0.001

Model trends are from 1960 to 1998. Correlation coefficients between model trends and observational trends from 1960 to 1998 and observational trends from 1950 to 1998 are shown.

Table 3. Area-Weighted Spatial Correlation Coefficients of Surface Air Temperature Trends Between Observations From 1950 to 1998 and Model Experiments From 1960 to 1998 for Each Hemisphere and Each Season

	Northern Hemisphere				Southern Hemisphere			
	DJF	MAM	JJA	SON	DJF	MAM	JJA	SON
Obs. versus GHGs	0.259	0.493	−0.007	−0.066	−0.051	0.216	−0.194	0.170
Obs. versus GHG1	0.105	0.213	−0.076	0.004	0.009	0.111	0.069	0.078
Obs. versus GHG2	0.288	0.518	0.064	−0.107	−0.053	0.119	−0.213	0.119
Obs. versus SO_4s	0.090	−0.056	0.062	−0.052	−0.069	0.114	−0.125	−0.056
Obs. versus $SO_4$1	−0.010	−0.027	0.094	0.059	−0.032	0.109	−0.029	−0.156
Obs. versus $SO_4$2	0.140	−0.062	0.017	−0.125	−0.064	0.048	−0.149	0.108

have been related to warming over Eurasia, cooling over Greenland, and decreasing sea level pressure over the Arctic. *Shindell et al*. [1999] found that recent changes in the AO were anthropogenic in origin in their model simulations and were most clearly manifested in models whose upper boundary is significantly above the tropopause and that allow a realistic simulation of the polar night vortex in the lower stratosphere. The present model has an upper boundary at 10 mbar. It, too, shows an increasing trend in the AO, but the amplitude is only one third of the observations (model T4G in Table 1 of *Shindell et al*. [1999] is similar to the current model). Over the past 30 years the AO appears to account for ~10% of the Northern Hemisphere variability in winter and 30% over Eurasia [*Thompson and Wallace*, 1998]. Over a 17-year time period ending in the mid-1990s, a related index, the North Atlantic Oscillation, was responsible for ~50% of the winter Northern Hemisphere extratropical temperature anomaly [*Hurrell*, 1996]. Were the model's AO response to have been stronger, it may have improved the spatial correlations with observed temperature trends, which is discussed next.

Table 1 shows, for each hemisphere and each season, the spatial correlation coefficients of temperature trends from 1960 to 1998 between observations and model experiments. In the Northern Hemisphere, positive correlations indicate that atmospheric composition forcing for the past 39 years exceeds regional climate variability there, except in summer. The GHG experiments indicate that the model is faithfully representing the real world's temperature changes in the Northern Hemisphere.

The ensemble of two simulations is helpful in reducing model noise. On the global average, spatial correlation coefficients in Table 1 between observations and the GHGs ensemble are greater than that between the observations and any single GHG experiment. Since the real world has only a single realization, even an excellent model would show correlation coefficients of the order of 0.3 to 0.5 according to *Wigley et al*. [1998].

In winter the model indicates that the greatest warming occurs in the Arctic Ocean. By the 1990s the winter sea ice cover in the GHGs ensemble covers 90.8% of the Arctic Ocean as opposed to 93.4% in the controls. Approximately 0.5°C of the model's area-weighted surface air temperature change is due to this greater open ocean area. In the observations, there is no station that was formerly on sea ice and is now on open water, so the greater open water effect is neglected. In fact, the observational data for the Arctic Ocean is not from sea ice stations at all but from interpolated land station data. The spatial correlation coefficients in the Northern Hemisphere are recalculated in Table 2 by excluding the Arctic Ocean. The correlations are stronger in Table 2 than in Table 1 in winter but weaker in spring and autumn.

Correlations between observations and GHG experiments are more strongly positive than those between observations and the GHG + SO_4 experiments. The increase since 1950 in net global radiation at the top of the atmosphere in the 1990s was 0.767 W m^{-2} for the GHGs ensemble but only 0.562 W m^{-2} for the GHG + SO_4s ensemble. Were this global radiative difference distributed proportionally to the normalized sulfate

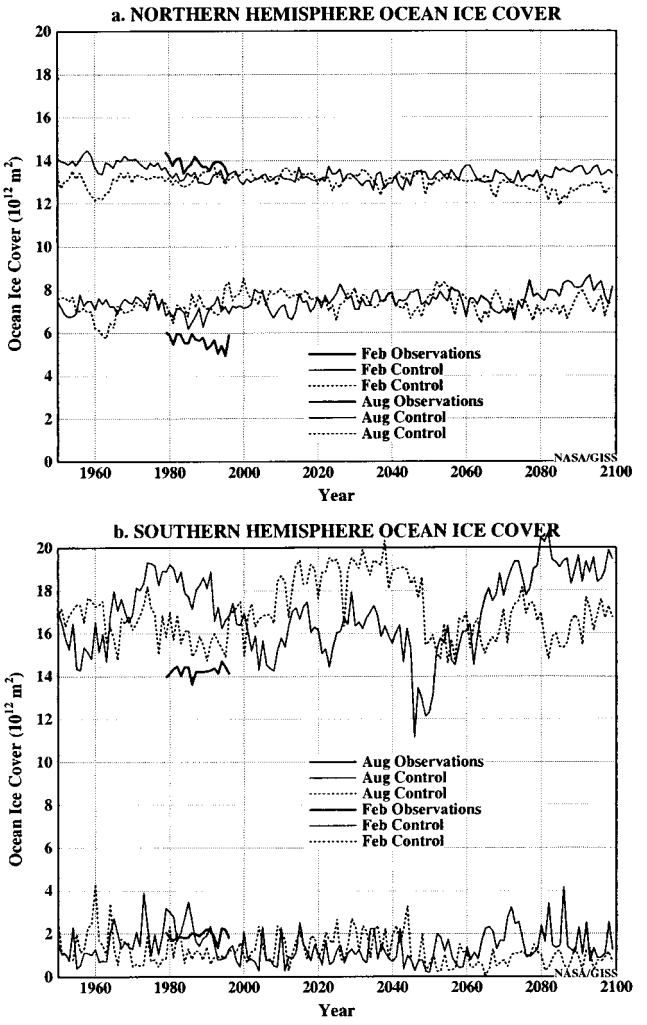

Figure 1. February and August hemispheric ocean ice cover (10^{12} m^2) for the satellite observations [*Cavalieri et al*., 1997] and the two control simulations.

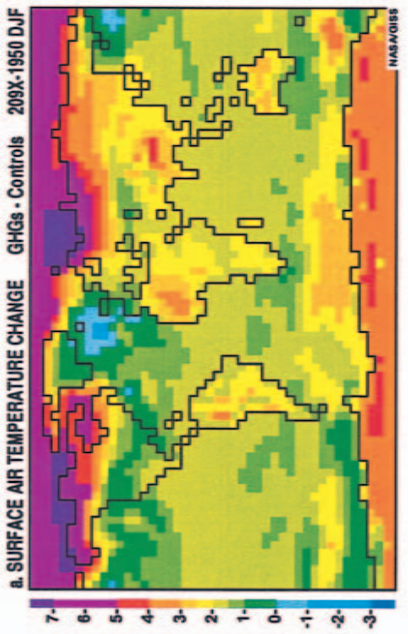

Plate 4. Winter and summer surface air temperature changes (°C) from 1950 to the 2090s for the GHGs ensemble minus the control simulations for the same decade.

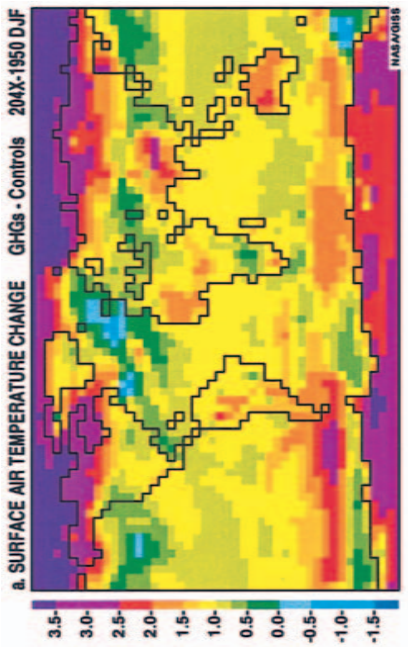

Plate 3. Winter and summer surface air temperature changes (°C) from 1950 to the 2040s for the GHGs ensemble minus the control simulations for the same decade.

loading pattern, some grid boxes in the GHG + SO_4 experiments would be losing 1 W m^{-2} as opposed to gaining 0.562 W m^{-2}. The actual strength and distribution of tropospheric aerosol forcing are uncertain, and what is added to the GHG + SO_4 experiments may be sufficiently inaccurate so as to degrade the spatial comparisons with observations. Note that the sulfate aerosols used here had a single scattering albedo of 1. Observations show that the real world's mixture of aerosols has a single scattering albedo between 0.9 and 0.95 [*Hansen et al*., 1998]. Thus, using sulfate aerosols exclusively may overestimate the cooling impact of aerosols which may have contributed to the degradation in our GHG + SO_4 results. Our conclusion with respect to sulfate aerosols is different from that obtained by *Mitchell et al*. [1995]. Although the ocean differences are quite small, the GHG + SO_4s ensemble shows, in winter, the largest cooling in eastern Siberia and warming in Hudson Bay and Baffin Bay which are contrary to the GHGs ensemble or to the observations of the past 39 years. One danger of adding aerosols of unknown strength and location is that they can be tuned to give more accurate comparisons with current observations but cover up model deficiencies.

The dependence of the observed temperature trends on the specific time period was examined by comparing 39-year trends with 49-year trends. There were no regions in the Northern Hemisphere with >1°C differences in summer and only three such regions in winter. Eastern United States and eastern Arctic Ocean showed significant cooling trends between 1950 and 1998, while Baffin Bay showed less cooling than in the 1960 to 1998 trends. The spatial correlation coefficients between the 49-year observed trends and the 39-year model trends are shown in Table 3. Much of the degradation in the correlations between Table 3 and Table 1 is due to the strong Arctic cooling in the 49-year observed trends. If the 49-year correlations are recalculated in the Northern Hemisphere by excluding the Arctic Ocean, then most of the strong positive correlations reappear as shown in Table 2. Recent evidence [*Rothrock et al*., 1999] indicates that Arctic sea ice has thinned by about 40% over the last few decades, which would also indicate a warming of sea ice temperature.

The lack of correlation and reduced impact of anthropogenic forcing during summer in the Northern Hemisphere should have been expected because the temperature signal is weakest in summer (compare Plates 2a and 2b). For both the model and observations, interannual variability over northern ocean areas is marginally greater in summer than in winter, which is consistent with the thinner mixed layer in summer. However, on land the interannual variability is smaller in summer for the model and smaller still for the observations. Deficiencies in the model's hydrologic cycle, which is more active in summer, may have degraded model results in summer. Root-mean-square differences between model and observed precipitation are nearly twice as large in summer than in winter over Northern Hemisphere land. Clouds and solar radiation are more important in summer than in winter.

In the Southern Hemisphere, negative correlations between the two GHG experiments or between the two GHG + SO_4 experiments indicate that the model's regional climate variability exceeds atmospheric composition forcing there. Part of this variability is due to sea ice cover. As discussed in section 5, the model's southern sea ice cover is stable, but its interannual variability is much greater than the observed variability. Thus the current model is not faithfully representing the real world's climate changes in the Southern Hemisphere, and it is unable to confirm whether atmospheric composition forcing for the past 39 years exceeds regional variability there.

The significance of the correlation coefficients shown in Tables 1–3 depends upon the spatial degrees of freedom of the surface air temperature trends. *Wang and Shen* [1999] estimated that for high-resolution temperature data the degrees of freedom are 60 in the Northern and 50 in the Southern Hemisphere for December–January–February and are 90 and 35 for June–July–August. We estimate that for a correlation coefficient to be significant at the 95% confidence level it must exceed 0.26 in the Northern Hemisphere and 0.28 in the Southern Hemisphere for December–January–February and exceed 0.21 and 0.34 for June–July–August.

5. Comparison of Model and Observed Sea Ice

Figure 1 shows the sea ice area for each hemisphere for February and August for the two control simulations and satellite observations [*Cavalieri et al*., 1997]. Sea ice in the control simulations is stable and has the proper seasonal variability. In the Northern Hemisphere it also has a realistic interannual variability, while in the Southern Hemisphere its interannual variability is much greater than that of the observations.

The model's excessive sea ice variability is a contributing factor that prevents the model from discerning a regional greenhouse signal in the Southern Hemisphere for 1960 to 1998. The modeled ocean structure below southern sea ice is almost isothermal and isohaline, in sharp contrast to the very shallow halocline overlying warmer, saltier water seen in the real world. We have identified two defects that may contribute to this problem. One is that the C grid scheme that solves the dynamical terms of the ocean momentum equations causes unrealistic alternating patterns of vertical mass transports particularly near the poles. This leads to unrealistic vertical mixing of water masses. The second defect is that sea ice rejects all salt when it is formed. This may cause stronger vertical mixing than is realistic.

6. Predicted Temperature Changes for the 2040s and 2090s

Plate 3 shows for winter and summer the predicted temperature changes from 1950 to the 2040s for the GHGs ensemble minus the control simulations. Plate 4 shows the temperature changes from 1950 to the 2090s. As discussed by *Russell and Rind* [1999], cooling continues to prevail in the North Atlantic associated with North Atlantic deep-water changes.

7. Conclusions

Interannual temperature variability is much smaller on a global scale than on a regional scale. Thus, for more than a decade, climate models have been able to simulate global temperature changes that matched observed changes. With the increasing time of anthropogenic climate forcing, regional temperature changes may have exceeded regional variability.

The NASA GISS atmosphere-ocean model has been used to simulate climate changes from 1950 to 2099. Two model GHG experiments from different initial states show large positive spatial correlations between themselves and with observations in simulating temperature changes of the past 39 years in the Northern Hemisphere except in summer. From this, we conclude that regional temperature changes forced by atmo-

spheric composition changes exceed regional temperature variability and the model is faithfully representing the real world in the Northern Hemisphere.

In the Southern Hemisphere, model experiments show inconsistent correlations between themselves and with the observations. The model's interannual variability of southern sea ice area significantly exceeds the observed variability. We deduce that the model is not faithfully representing the real world in the Southern Hemisphere, and we cannot confirm that the regional greenhouse signal has been detected there. (Additional plots and additional quantities of these simulations along with the atmosphere-ocean model code, are available at our web site: http://aom.giss.nasa.gov.)

Acknowledgments. The authors wish to thank James E. Hansen for his support in the atmosphere-ocean model development at GISS, for the use of his temperature data, and for his comments of this manuscript.

References

Abramopoulos, F., C. Rosenzweig, and B. Choudhury, Improved ground hydrology calculations for global climate models (GCMs): Soil water movements and evapotranspiration, *J. Clim*., *1*, 921–941, 1988.

Cavalieri, D. J., C. L. Parkinson, P. Gloersen, and H. J. Zwally, Arctic and Antarctic sea ice concentrations from multichannel passive-microwave satellite data sets: October 1978 to September 1995, user's guide, *NASA Tech. Memo*., *TM-104627*, 17 pp., 1997.

Delworth, T. L., and T. R. Knutson, Simulation of early 20th century warming, *Science*, *287*, 2246–2250, 2000.

Hansen, J., G. Russell, A. Lacis, I. Fung, D. Rind, and P. Stone, Climate response times: Dependence on climate sensitivity and ocean mixing, *Science*, *229*, 857–859, 1985.

Hansen, J., I. Fung, A. Lacis, D. Rind, S. Lebedeff, R. Ruedy, and G. Russell, Global climate changes as forecast by Goddard Institute for Space Studies three-dimensional model, *J. Geophys. Res*., *93*, 9341–9364, 1988.

Hansen, J., R. Ruedy, and M. Sato, Global surface air temperature in 1995: Return to pre-Pinatubo level, *Geophys. Res. Lett*., *23*, 1665–1668, 1996.

Hansen, J. E., M. Sato, A. Lacis, R. Ruedy, I. Tegen, and E. Matthews, Climate forcings in the industrial era, *Proc. Natl. Acad. Sci. U.S.A*., *95*, 12,753–12,758, 1998.

Hansen, J., R. Ruedy, J. Glascoe, and M. Sato, GISS analysis of surface temperature change, *J. Geophys. Res*., *104*, 30,997–31,022, 1999.

Houghton, J. T., L. G. Meira Filho, J. Bruce, H. Lee, B. A. Callander, E. Haites, N. Harris, and K. Maskell (Eds.), *Climate Change 1994*, 339 pp., Cambridge Univ. Press, New York, 1994.

Hurrell, J. W., Influence of variations in extratropical wintertime teleconnections on Northern Hemisphere temperature, *Geophys. Res. Lett*., *23*, 665–668, 1996.

Knutson, T. R., T. L. Delworth, K. W. Dixon, and R. J. Stouffer, Model assessment of regional surface temperature trends (1947–1997), *J. Geophys. Res*., *104*, 30,981–30,996, 1999.

Large, W. G., J. C. McWilliams, and S. C. Doney, Oceanic vertical mixing: Review and a model with non-local boundary layer parameterization, *Rev. Geophys*., *32*, 363–403, 1994.

Levitus, S., R. Burgett, and T. P. Boyer, *World Ocean Atlas 1994*, U.S. Dep. of Commer., Natl. Oceanic and Atmos. Admin., Silver Spring, Md., 1994.

Miller, J. R., and G. L. Russell, Investigating the interactions among river flow, salinity and sea ice using a coupled atmosphere-ocean-ice model, *Ann. Glaciol*., *25*, 121–126, 1997.

Mitchell, J. F. B., R. A. Davis, W. J. Ingram, and C. A. Senior, On surface temperatures, greenhouse gases and aerosols: Models and observations, *J. Clim*., *8*, 2364–2386, 1995.

Rothrock, D. A., Y. Yu, and G. A. Maykut, Thinning of the Arctic sea-ice cover, *Geophys. Res. Lett*., *26*, 3469–3472, 1999.

Russell, G. L., and D. Rind, Response to CO_2 transient increase in the GISS coupled model: Regional coolings in a warming climate, *J. Clim*., *12*, 531–539, 1999.

Russell, G. L., J. R. Miller, and D. Rind, A coupled atmosphere-ocean model for transient climate change studies, *Atmos. Ocean*, *33*(4), 683–730, 1995.

Shindell, D. T., R. L. Miller, G. A. Schmidt, and L. Pandolfo, Simulation of recent northern winter climate trends by greenhouse-gas forcing, *Nature*, *339*, 452–455, 1999.

Tett, S. F. B., P. A. Stott, M. R. Allen, W. J. Ingram, and J. F. B. Mitchell, Causes of twentieth-century temperature change near the Earth's surface, *Nature*, *399*, 569–572, 1999.

Thompson, D. W. J., and J. M. Wallace, The arctic oscillation signature in the wintertime geopotential height and temperature fields, *Geophys. Res. Lett*., *25*, 1297–1300, 1998.

Wang, X., and S. S. Shen, Estimation of spatial degrees of freedom of a climate field, *J. Clim*., *12*, 1280–1291, 1999.

Wigley, T. M. L., P. J. Jaumann, B. D. Santer, and K. E. Taylor, Relative detectability of greenhouse-gas and aerosol climate change signals, *Clim. Dyn*., *14*, 781–790, 1998.

J. R. Miller, D. Rind, R. A. Ruedy, G. L. Russell, G. A. Schmidt, and S. Sheth, NASA Goddard Institute for Space Studies, 2880 Broadway, New York, NY 10025. (grussell@giss.nasa.gov)

(Received August 13, 1999; revised January 6, 2000;
accepted February 28, 2000.)